Experimental and numerical investigation of contact heat transfer between a rotating heat pipe and a steel strip

Celik, Metin; Devendran, Kathikeyan; Paulussen, Geert; Pronk, Pepijn; Frinking, Ferry; de Jong, Wiebren; Boersma, Bendiks J.

DOI
10.1016/j.ijheatmasstransfer.2018.02.009

Publication date
2018

Document Version
Final published version

Published in
International Journal of Heat and Mass Transfer

International Journal of Heat and Mass Transfer 122 (2018) 529–538

Contents lists available at ScienceDirect

International Journal of Heat and Mass Transfer

journal homepage: www.elsevier.com/locate/ijhmt

Experimental and numerical investigation of contact heat transfer between a rotating heat pipe and a steel strip

Metin Celik [a,*], Karthikeyan Devendran [a], Geert Paulussen [b], Pepijn Pronk [b], Ferry Frinking [b], Wiebren de Jong [a], Bendiks J. Boersma [a]

[a] Process & Energy Department, Faculty of Mechanical, Maritime and Materials Engineering, Delft University of Technology, The Netherlands
[b] Research & Development, Tata Steel, IJmuiden, The Netherlands

ARTICLE INFO

Article history:
Received 27 September 2017
Received in revised form 7 December 2017
Accepted 4 February 2018
Available online 8 February 2018

Keywords:
Contact heat transfer
Experimental validation
Gas entrainment
Numerical model
Rotating heat pipe

ABSTRACT

A new concept for energy efficient annealing of steel strip comprises of multiple rotating heat pipes. Each heat pipe extracts heat from the cooling strip which is reused to increase the temperature of the heating strip. In this context, the heat transfer between the steel strip and the rotating heat pipe is investigated. When the strip is transported over the heat pipe, gas entrains in the gap. The gas compresses into a uniform gas layer. The contact heat transfer deteriorates due to this phenomenon. A numerical model to quantify the heat transfer between the surfaces is developed. Since there is no direct way to quantify the heat transfer between two moving surfaces, the problem is divided into a gas entrainment and a heat transfer part. The model is validated with experiments executed on a rotating heat pipe test rig. The validation was made varying the strip thickness, specific tension and strip velocity. The results show a uniform gas layer forming within the first 1° of the 180° wrap angle in all cases. The heat transfer is dominated by gas conduction. Results for the uniform gas layer region yield heat transfer coefficients in the range between 4000 and 20,000 $W/m^2 \cdot K$.

1. Introduction

Cold rolling of steel causes an increase in the hardness of the material. In order to restore its ductility, the steel is heated to approximately 700 °C and cooled down to ambient temperature. This energy intensive process is called annealing and is an essential heat treatment process in the steel industry [1]. In a conventional process, none of the applied energy is retained in the product.

Therefore, an alternative technology was developed to reuse the heat extracted during the cooling of the strip in the heating part of the cycle. In this concept, the strip being cooled is thermally linked to the strip being heated with rotating heat pipes [2].

A heat pipe is a highly efficient heat transfer device. It is a closed pipe which contains a fixed amount of working fluid. This working fluid carries the heat from one end to the other by means of evaporation, vapor transport and condensation [3]. In order to work continuously, the condensed liquid needs to be driven back to the evaporation zone. The method used to transport the liquid varies among different types of heat pipes [4, 5]. For rotating heat pipes, this is accomplished by the centrifugal force produced by the rotation of the heat pipe around its symmetric axis [6,7].

Thanks to the high efficiency of the heat pipes, the alternative annealing technology promises a reduction of energy consumption of up to 70% [2]. To implement this technology, the contact heat transfer between the rotating heat pipe and the steel strip needs to be thoroughly investigated.

When a strip is transported over a roll, gas is dragged in between these two surfaces. The gas compresses and forms a stable thin gas layer over the wrap angle. The gas layer forms a thermal resistance between the strip and the roll, thus limiting the heat transfer from one to the other. The thickness of a gas layer between two surfaces moving at relative speed has been extensively studied in the context of foil bearings. However, these studies do not consider heat transfer between the surfaces and do not describe cases where relative motion is zero or near zero.

In the foil bearing studies, it has been observed that, with the exception of inlet and outlet region, a uniform gas layer thickness forms when the foil tension and the wrap angle are sufficiently large [8,9]. Therefore, the work on foil bearings divides the problem into an inlet and outlet region. This approach allows for an asymptotic convergence of the inlet and outlet regions to the

* Corresponding author at: TU Delft, Process & Energy Department, Leeghwaterstraat 39, 2628 CB Delft, The Netherlands.
E-mail address: M.Celik@tudelft.nl (M. Celik).

https://doi.org/10.1016/j.ijheatmasstransfer.2018.02.009
0017-9310/

Nomenclature

C	compressibility parameter
C^*	normalized compressibility parameter
c_p	specific heat, J/kg·K
D	bending stiffness per unit width, N·m
h	gas layer thickness, m
H	dimensionless gas layer thickness
H^*	dimensionless gas layer thickness in uniform region
$\bar{H}$	normalized gas layer thickness
H_e	Vickers hardness, Pa
k_g	thermal conductivity of gas, W/m·K
k_s	harmonic thermal conductivity, W/m·K
K	integration constant
m	slope of roughness peaks
p	gas layer pressure, Pa
p_a	ambient pressure, Pa
p_c	contact pressure, Pa
p_m	pressure required for full contact, Pa
R	arc of curvature, m
r_o	roll radius, m
Ra	surface roughness, m
Ra_e	effective roughness, m
s	coordinate along the wrap angle direction
S	stiffness parameter
$\bar{S}$	normalized stiffness parameter
t	strip thickness, m
T	temperature, K
T_s	strip specific tension, Pa
U	velocity of the strip, m/s
υ	velocity of the node, m/s
z	radial coordinate
$\mathcal{Z}$	radial distance to the node, m
α_{total}	overall heat transfer coefficient, W/m^2·K
α_{solid}	solid contact heat transfer coefficient, W/m^2·K
α_{gas}	gas conduction heat transfer coefficient, W/m^2·K
α_{rad}	radiation heat transfer coefficient, W/m^2·K
β	perturbation parameter
ε	emissivity
θ	angular coordinate
μ	viscosity, Pa·s
ξ	extended coordinate
$\bar{\xi}$	normalized extended coordinate
ρ	density, kg/m^3
σ	Stefan-Boltzmann constant, W/m^2·K^4
Φ	dimensionless pressure

uniform gas layer thickness. A base for infinitely wide and perfectly flexible foil is given in [10]. The foil stiffness is described in [11] and integrated in [12]. The numerical solution for compressing the gas layer is provided in [13]. A review of these studies is provided in [14].

For the specific case where the tension of the foil and the wrap angle is small, the problem can be solved at once, without dividing it into an inlet and an outlet branch. This method also allows for the tension change due to friction between the foil and the roll over the wrap angle. Such a method is described in [15–20]. In these studies, the foil is in physical contact with the roll.

In addition to the determination of the gas layer thickness, the heat transfer between two macroscopically conforming surfaces should be studied for the problem at hand. Heat transfer between two rough surfaces is divided into the heat transfer across the gas gap and the heat transfer through solid contact in [21]. In this extensive study, the complexity of the gap geometry is overcome by simplifying the gap heat transfer as the heat transfer between the projected surfaces. The solid heat transfer is determined using a correlation including contact pressure, surface parameters and thermal conductivities. Results of analytical and experimental studies for the thermal resistance of gases are given in [22]. In [23], the thermal gap conductance is experimentally studied and good agreement is obtained with theory. A comprehensive review of the subject is made in [24].

The experimental investigation of contact heat transfer between a strip and a roll has not been widely addressed so far. In [25] and [26], such a study is performed in a dedicated roll regenerative furnace. In that study, a hollow shell is used as the roll and the strip velocities are relatively low. The contact heat transfer coefficient values reported in [26] are used in the modelling of a multi-roll heat exchanger with two strips moving in opposite direction in [27].

The current study aims to model and experimentally investigate the heat transfer between a steel strip and a rotating roll. In the modelling part of this work, a novel methodology for quantifying the heat transfer is adopted. Since there is no straightforward way to calculate the heat transfer between two moving surfaces, the problem is divided into a gas entrainment and a heat transfer part. The gas layer thickness between the two surfaces is found with an asymptotic approach, incorporating the stiffness of the strip, the contact between the surfaces and the compressibility of the gas. The model therefore is a combination of the approaches found in [12], [13] and [16]. However, the derivation of the governing equations is somewhat different. The solution for gas layer and contact pressure is coupled with the contact heat transfer model described in [21]. With this combination, the contact heat transfer coefficient evolution along the wrap angle is found.

The experimental part of the current work is performed on a test rig comprising of a roll executed as a heat pipe over which a steel strip travels. The temperature evolution of the steel strip as it travels over the wrap angle is measured at various strip velocity, strip tension and strip thickness configurations. During the measurements, the behavior of the heat pipe is also tracked. As opposed to previous work in literature, the use of a heat pipe in the validation process allows for better isolation of the heat transfer between the strip and the roll from outside influence. This is the case because it allows for a Dirichlet boundary condition at the interior of the roll.

The modelling and experimental results are reported for various configurations of strip velocity, tension and thickness. Such a catalogue of contact heat transfer coefficients also sheds light on the parameters affecting the heat transfer for similar applications.

2. Problem modelling

The analysis for the steel strip transported over a rotating heat pipe is simplified to the study of a strip traveling over a roll. The infinitely wide strip travels at velocity U and is tensioned with T_s over the roll radius r_o. The heat pipe is considered to be non-deformable whereas the strip can bend depending on the forces acting on it. As the heat pipe is freely suspending, its velocity is assumed to be equal to the velocity of the strip. The absolute pressure of the gas layer is p and its thickness is h. The wrap angle is divided into three regions; namely the inlet region (A), the uniform region (B) and the outlet region (C). Tension on the strip is applied some distance away from the roll marked as (D) (see Fig. 1).

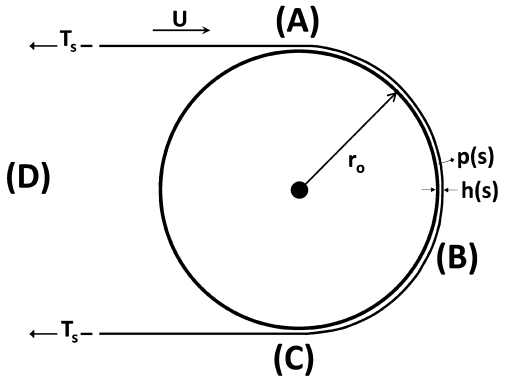

Fig. 1. Simplified view of the system.

Taking s as the coordinate along the direction of the wrap angle, the general form of the steady state Reynolds lubrication equation is written as in Eq. (1):

$$\frac{d}{ds}\left(h^3 p\frac{dp}{ds}\right) = 12\mu U\frac{d(ph)}{ds} \tag{1}$$

where μ is the dynamic viscosity of the gas.

In order to solve the force equilibrium at constant speed, a balance equation for the strip is described in Eq. (2) [11]:

$$D\frac{d^4h}{ds^4} = p + p_c - p_a - \frac{T_s t}{R} \tag{2}$$

where D is the bending stiffness per unit width, p_c is the contact pressure, p_a is the ambient pressure, t is the strip thickness, R is the arc of curvature of the strip and T_s is the strip specific tension. Contact pressure is described as a function of the distance between the strip and the roll surfaces, h, with an empirical relation as seen in Eq. (3) [16]:

$$p_c = \begin{cases} 0 & h > Ra_e \\ \left(\frac{\sqrt{p_m}}{Ra_e}(Ra_e - h)\right)^2 & h \leqslant Ra_e \end{cases} \tag{3}$$

where p_m is the pressure required to force h to zero[1] and Ra_e is the effective roughness of the two surfaces. The effective roughness Ra_e is calculated with Eq. (4) [21].

$$Ra_e = \sqrt{Ra_1 + Ra_2} \tag{4}$$

where Ra_1 and Ra_2 are the roughness values of the involved surfaces. The curvature is described as in Eq. (5), when $h<<<r_o$ [13]:

$$\frac{1}{R} = \frac{1}{r_o} - \frac{d^2h}{ds^2} \tag{5}$$

Differentiating Eq. (2) and combining it with Eq. (5), the derivative of p is found as shown in Eq. (6):

$$\frac{dp}{ds} = D\frac{d^5h}{ds^5} - T_s t\frac{d^3h}{ds^3} \tag{6}$$

Combining Eqs. (6), (1) and (2), the governing equation Eq. (7) is obtained:

$$\frac{d}{ds}\left(h^3 p\left(D\frac{d^5h}{ds^5} - T_s t\frac{d^3h}{ds^3}\right)\right) = 12\ \mu U\frac{d(ph)}{ds} \tag{7}$$

[1] The value for p_m is taken as 281 MPa for stainless steel AISI 316 [28]. Although the materials used during the experiments are low carbon steel for strip and stainless steel AISI304 for the roll (Table 2), the p_m value for a combination of these materials was not available.

The governing equation is worked into a different form introducing the following dimensionless parameters shown in Eqs. (8)--(13) [12,13]:

$$\beta = \frac{12\ \mu U}{T_s t} \tag{8}$$

$$H = \frac{h\beta^{-2/3}}{r_o} \tag{9}$$

$$C = \frac{p_a - p_c}{(T_s t)/r_o} \tag{10}$$

$$S = \frac{D\beta^{-2/3}}{(T_s t)r_o^2} \tag{11}$$

$$\Phi = \frac{p - p_a + p_c}{(T_s t)/r_o} \tag{12}$$

$$\xi = \frac{s\beta^{-1/3}}{r_o} \tag{13}$$

where β is chosen as a perturbation parameter. It has a different constant value for each considered case and it is closely related to the gas layer thickness at the uniformity region [9]. The compressibility effects are represented by the compressibility parameter C. As the ambient pressure dominates over the force applied by the strip tension to the heat pipe, $1/C$ is expected to approach zero. Consequently, this converts the problem to an incompressible one [13]. S is the stiffness parameter, representing the ratio of the moment required to bend the strip to a radius of curvature of r_o and the moment of the strip tension about the center of the heat pipe [12]. H is the dimensionless gap, ϕ is the dimensionless pressure and ξ is an extended coordinate introduced to ensure consistent differentiation of other parameters. $\xi = 0$ corresponds to the initial and final point of contact of a perfectly flexible foil at the stationary situation, whereas ξ approaches $-\infty$ in the uniform region (B) and ∞ beyond the arc of contact. The selection of the powers 1/3 and 2/3 are made in a way that the β values are eliminated from the final equation to be derived.

The dimensionless parameters are used to convert Eqs. (7)--(14):

$$\frac{d}{ds}\left(H^3(\Phi + C)\left(S\frac{d^5H}{d\xi^5} - \frac{d^3H}{d\xi^3}\right)\right) = \frac{d}{ds}(H(\Phi + C)) \tag{14}$$

Integration of Eq. (14) leads to Eq. (15):

$$H^3(\Phi + C)\left(S\frac{d^5H}{d\xi^5} - \frac{d^3H}{d\xi^3}\right) = H(\Phi + C) + K \tag{15}$$

where K is the integration constant. At the uniform region, as the gas layer thickness becomes constant, the derivatives of h and thus H, converge to zero. Therefore, when ξ nears $-\infty$ (uniform region), the left-hand side of Eq. (15) approaches zero. The right-hand side is worked out by writing ϕ in terms of the derivatives of H by combining Eqs. (2), (5) and (12), resulting in Eq. (16):

$$\Phi = S\frac{d^4H}{d\xi^4} + 1 - \frac{d^2H}{d\xi^2} \tag{16}$$

With this form, when ξ nears $-\infty$, it is clear that ϕ approaches 1. This gives the integration constant shown in Eq. (17):

$$K = -H^*(1 + C) \tag{17}$$

where H^* is defined as the dimensionless gas layer thickness at the uniform region. The resulting governing equation is therefore described with Eq. (18):

$$H^3\left(S\frac{d^4H}{d\xi^4}+1-\frac{d^2H}{d\xi^2}+C\right)\left(S\frac{d^5H}{d\xi^5}-\frac{d^3H}{d\xi^3}\right) = H\left(S\frac{d^4H}{d\xi^4}+1-\frac{d^2H}{d\xi^2}+C\right)-H^*(1+C) \quad (18)$$

The defined dimensionless parameters in Eqs. (8) -- (13) can be normalized with the dimensionless gas layer thickness at the uniform region H^*, resulting in Eqs. (19) -- (22) [12,13]:

$$\bar{H}=\frac{H}{H^*} \quad (19)$$

$$\bar{\xi}=\frac{\xi}{H^*} \quad (20)$$

$$\bar{S}=\frac{S}{H^{*2}} \quad (21)$$

$$C^*=(1+C)H^* \quad (22)$$

Using these normalized terms, Eq. (18) can be worked into Eq. (23):

$$\bar{S}\frac{d^5\bar{H}}{d\bar{\xi}^5}-\frac{d^3\bar{H}}{d\bar{\xi}^3}=\pm\frac{\bar{H}-\frac{C^*}{\bar{S}\frac{d^4\bar{H}}{d\bar{\xi}^4}-\frac{d^2\bar{H}}{d\bar{\xi}^2}+C^*}}{\bar{H}^3} \quad (23)$$

The ± sign in Eq. (23) represents different equations for the inlet (+) and outlet regions (−). Towards the uniform region (B), $\bar{H}$ converges to 1 and its derivatives to 0. On the other hand, towards region (D), the gas layer thickness increases and the strip approaches a straight shape. This geometry requires the convergence of $\bar{H}'$ to $\bar{\xi}$ H^* far away from the roll [13]. This also implies that $\bar{H}''$ asymptotically approaches H^*. The boundary conditions are summarized in Table 1.

These boundary conditions are used to solve the 5th order ODE in Eq. ((23) as a boundary value problem) with MATLAB®. Air properties are obtained from FluidProp® at the average temperature of the strip and the heat pipe [29].

Through the solution of the above ODE, the thickness and the pressure distribution of the gas layer, the contact pressure as well as the extent of regions (A), (B) and (C) can be determined.

The heat transfer coefficient α at the uniform region (B) is calculated by the addition of individual contributions as shown in Eq. (24) [21].

$$\alpha_{total}=\alpha_{solid}+\alpha_{gas}+\alpha_{rad} \quad (24)$$

where α_{total} represents the heat transfer coefficient between the strip and the outer surface of the roll.

The surface fractions of the heat transfer coefficients in Eq. (24) are incorporated in their respective descriptions. The solid contact heat transfer area is a very small fraction of the total heat transfer area. As a result, the heat transfer area through gas is almost equal to the total heat transfer area. The solid contact heat transfer coefficient is calculated with Eq. (25) which is already based on the solid contact surface fraction [21]:

Table 1
Boundary conditions for the model.

Boundary conditions	
$\bar{\xi}\to-\infty$	$\bar{H}\sim 1$
$\bar{\xi}\to-\infty$	$\bar{H}'\sim 0$
$\bar{\xi}\to-\infty$	$\bar{H}''\sim 0$
$\bar{\xi}\to\infty$	$\bar{H}'\sim \bar{\xi}$ H*
$\bar{\xi}\to\infty$	$\bar{H}''\sim$ H*

$$\alpha_{solid}=1.25\frac{k_s m}{Ra_e}\left[\frac{p_c}{H_e}\right]^{0.95} \quad (25)$$

where k_s is the harmonic thermal conductivity of the surfaces, m is the slope of roughness peaks and H_e is the Vickers hardness of the strip.

The heat transfer through gas, on the other hand, occurs via conduction. Natural convection is ignored as the $Gr/Re^2 < 1$, with Gr being the Grashof number and Re being the Reynolds number. The Knudsen number is less than 0.1 for all simulated cases, therefore the flow is in a continuum regime [22]. Consequently, the heat transfer coefficient through the gas layer is calculated with Eq. (26) [23]:

$$\alpha_{gas}=\frac{k_g}{h} \quad (26)$$

where k_g is the thermal conductivity of the gas.

The heat transfer coefficient for radiation is modelled with the radiation taking place between two gray parallel plates, as shown in Eq. (27) [30]:

$$\alpha_{rad}=\frac{\sigma(T_1^4-T_2^4)}{\left(\frac{1}{\varepsilon_1}+\frac{1}{\varepsilon_2}-1\right)(T_1-T_2)} \quad (27)$$

where T_1 and T_2 are the temperatures of the surfaces, ε_1 and ε_2 are the emissivities of the surfaces and σ is the Stefan-Boltzmann constant.

With these equations, the thickness of the gas layer, the gas layer pressure, the contact pressure and the heat transfer are described.

3. Experiments

3.1. Experimental facilities

The experimental setup used in this work is a rotating heat pipe with integrated steel strips built as the proof of principle of the heat pipe assisted annealing concept (see Fig. 2). It was developed to study the combined heat transfer from the strip to the interior of the heat pipe, through the conducting heat pipe shell and from the inner surface of the heat pipe to the heat pipe working fluid. The steel strips are tensioned between the rotating heat pipe and auxiliary rolls with pneumatic cylinders. Induction is used to heat one of the strips (see Fig. 3).

The heat pipe uses demineralized water as working fluid. Its operating temperature ranges from ambient temperature to 120 °C. The strip that is heated by induction is fed to the evaporator section of the heat pipe and cools down as it transfers its heat to

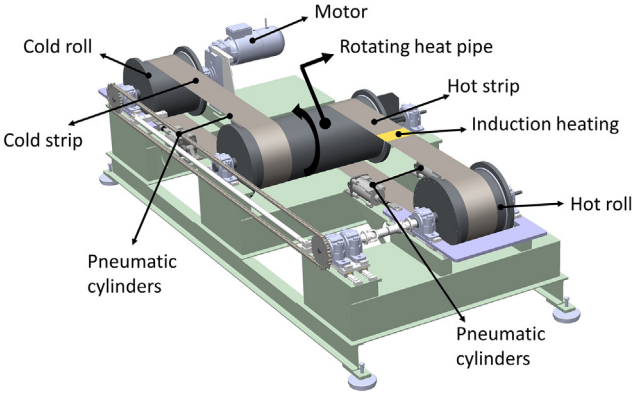

Fig. 2. CAD view of the experimental setup.

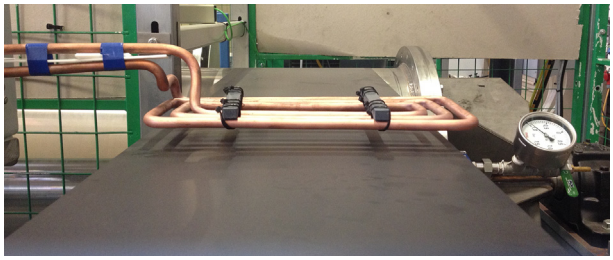

Fig. 3. Strip heating with induction.

the heat pipe. The working fluid evaporates causing a local pressure increase. The increased pressure drives the vapor towards the condenser where it condenses. During condensation heat is released, which is picked up by the cold strip. The liquid is driven back to the evaporator by means of centrifugal force and the head that is formed by evaporation and condensation. The specifications of the setup are given in Table 2.

In order to study the contact heat transfer between the steel strip and the rotating heat pipe, the temperature evolution of the strip as it is being cooled is recorded with an infrared camera. The infrared camera is aimed at the first 45° of the wrap angle (see Fig. 4). The infrared camera is a Cedip Jade 3 medium Wave camera 3–5 μm with a 50 mm lens and Sofradir MCT 320 × 240 pixel chip. It is set to record 2 frames per second. The steel strip is coated with an organic heat resistant coating to improve its emissivity for the wavelength employed by the infrared camera. Additionally, the temperature inside the heat pipe is measured with a K-type thermocouple placed in the vapor channel. The system is driven by a frequency controlled drive with an encoder control loop. The strip tension is applied by pneumatic cylinders, of which the pressure is set and logged. Applying the strip tension with pneumatic cylinders ensures that the total tension over both strip legs is maintained at any temperature. The sensor signals are recorded with a data logger every 3 s.

3.2. Methodology

A summary of the experimental plan is given in Fig. 5. The parameters that are varied for the experiments are strip velocity, strip thickness and strip tension. In total, 29 cases are examined.

For each experiment, a near steady state is reached before recording the measurements. Each measurement is taken for a duration of 30 s, resulting in a video of 60 frames for the infrared camera and 10 data points for the other readings. The digital level

Table 2
Setup specifications.

Parameter	Data
Strip material	Cold rolled low carbon steel
Strip gauge	0.26 mm/0.35 mm
Strip width	300 mm
Strip roughness (Ra)	0.37 μm
Heat pipe material	Stainless steel AISI 304
Heat pipe outer diameter	502 mm
Heat pipe wall thickness	6.5 mm
Heat pipe length	1210 mm
Heat pipe roughness (Ra)	0.75 μm
Water amount inside heat pipe	2 kg (1% fill ratio)
Maximum strip velocity	8 m/s
Maximum strip tension	69 MPa for 0.26 mm strip 52 MPa for 0.35 mm strip
Induction unit capacity	50 kW_e
Induction coil geometry	Rectangular loop of 28.8 × 14.5 cm with 3 windings

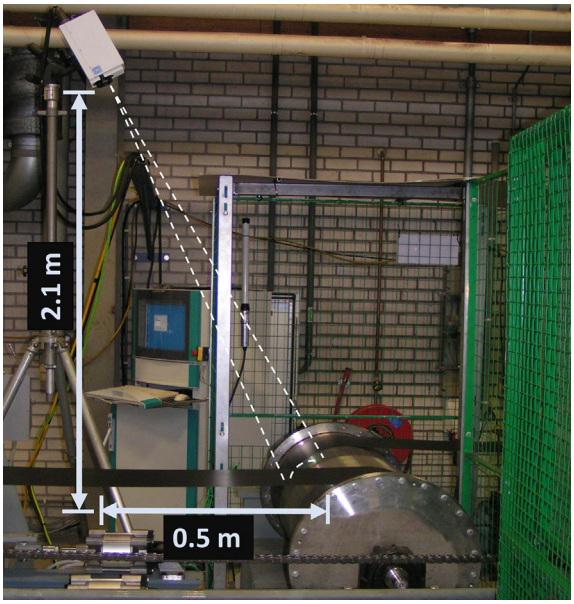

Fig. 4. Measurements on the experimental setup.

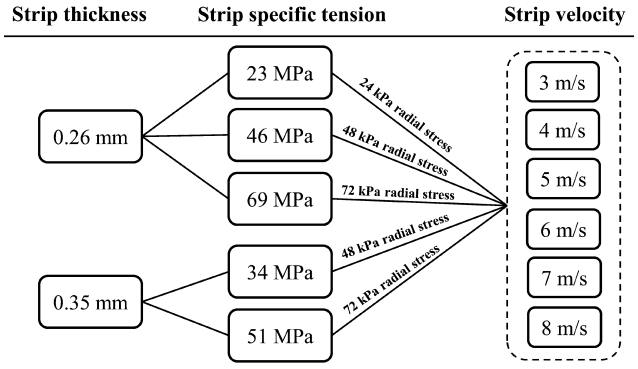

Fig. 5. Experimental plan. *The data point for 0.26 mm/69 MPa/5 m/s is not available.

readings from the infrared camera are converted to temperature readings with Wien's approximation of Planck's law for short wavelengths [31]. The camera results are compensated for the changing angle of the observed strip. The data was analyzed to determine if near steady state was actually reached and to determine the measurement precision.

Because the heat transfer coefficient and the gas gap cannot be directly measured, the descriptions are integrated into a system model describing the strip and the evaporator side of the heat pipe in the test setup. The model is a 2D, steady state, finite difference model, describing the heat pipe evaporator, the heat pipe shell and the strip wrapped around it (see Fig. 6).

In the finite difference model, the strip is meshed only in the angular direction, as the relevant Biot number is less than 0.1. The roll, on the other hand, is meshed in both the angular and the radial directions. All the nodes are solved using a steady state energy balance. The energy balance equation for an arbitrary node is shown in Eq. (28):

$$0 = \rho c_p \upsilon \frac{1}{\mathcal{Z}} \frac{\partial T}{\partial \theta} + \frac{1}{\mathcal{Z}} \frac{\partial}{\partial \theta} \left(k \frac{1}{\mathcal{Z}} \frac{\partial T}{\partial \theta} \right) + \frac{\partial}{\partial z} \left(k \frac{\partial T}{\partial z} \right) \tag{28}$$

where ρ is the density, c_p is the specific heat capacity, k is the thermal conductivity, υ is the velocity of the node, $\mathcal{Z}$ is the distance

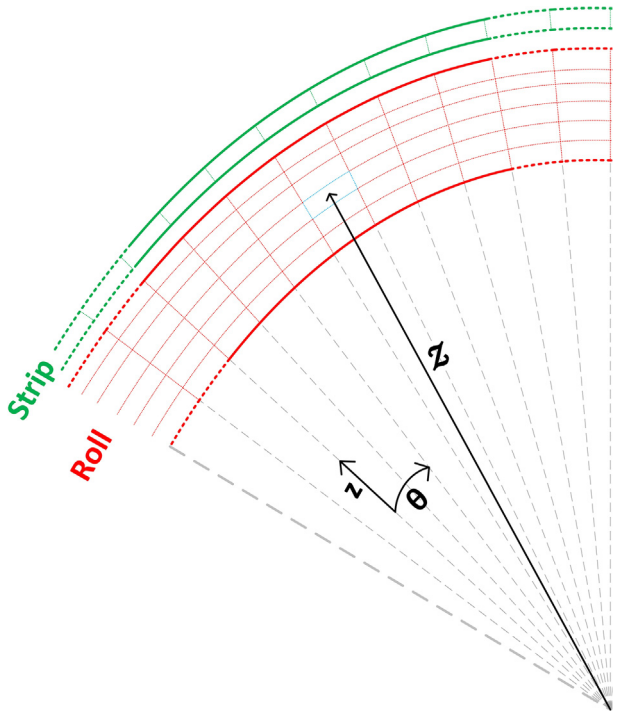

Fig. 6. Finite difference model layout.

from the center of the roll to the node and T is the temperature of the node. The angular coordinate is θ, whereas the radial coordinate is z.

Eq. (28) is integrated over the nodes. The equations are discretized with the hybrid differencing scheme, which uses upwind differencing for Péclet number values of $\geq$2 and switches to central differencing scheme for Péclet number values of <2 [32]. The heat losses from the strip and the outer surface of the roll to the environment as well as the strip / roll interaction and the fixed vapor channel temperature inside the roll are imposed as boundary conditions.

Inputs to this model are the evaporator temperature, the strip velocity and the inlet strip temperature. The output of the model is the temperature evolution for the strip along the wrap angle. The actual heat transfer coefficient is sought by iterative adjustment of the modelled heat transfer coefficient. The iteration objective is the minimization of least squares of the strip temperature evolution along the observed arc of contact (see Fig. 7).

3.3. Uncertainty analysis

An uncertainty analysis is made for the found heat transfer coefficients. The experimental parameters that contribute to the uncertainty of the results are the uncertainty of the temperature readings from the thermocouple inside the heat pipe and the temperature readings from the infrared camera. Additionally, the uncertainties in the parameters used in the system model were examined [33] leading to the inclusion of the evaporation heat transfer coefficient (taken as 4000 W/m^2·K [34] during the data processing) into the uncertainty analysis.

The experimental results are presented along with a 95% confidence interval. All the measured effects are attributed to variations in the actual heat transfer coefficient. It is observed that the uncertainty in the experimental results is much smaller for the cases where the thermal resistance between the strip and the roll is dominant (low contact heat transfer coefficient cases). For situations where this thermal resistance is low, uncertainty rapidly increases to very large values. This is because what is actually measured during the experiments is the overall thermal resistance of the system rather than the contact thermal resistance. The contact thermal resistance is however calculated from this overall thermal resistance. The contribution of a low contact thermal resistance to the overall thermal resistance of the system (the contact, the heat pipe shell and the evaporation thermal resistances) is low and insensitive since the total resistance will be governed by the other resistances. This insensitivity results in a large uncertainty in the determination of the contact resistance.

Consequently, it is noted that the cases with lower heat transfer coefficients between the strip and the roll have a lower uncertainty (see Figs. 8–10).

4. Results

4.1. Validation

The contact heat transfer coefficient depends on strip velocity, radial stress and gas properties. The heat transfer coefficients derived from the experiments and the model are given in

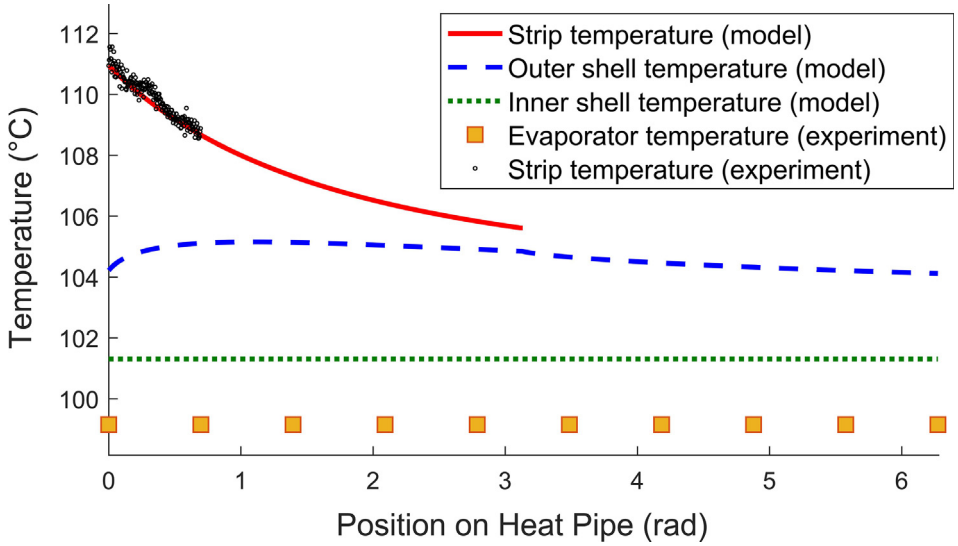

Fig. 7. Example case with the data processing model (0.26 mm/23 MPa/3 m/s).

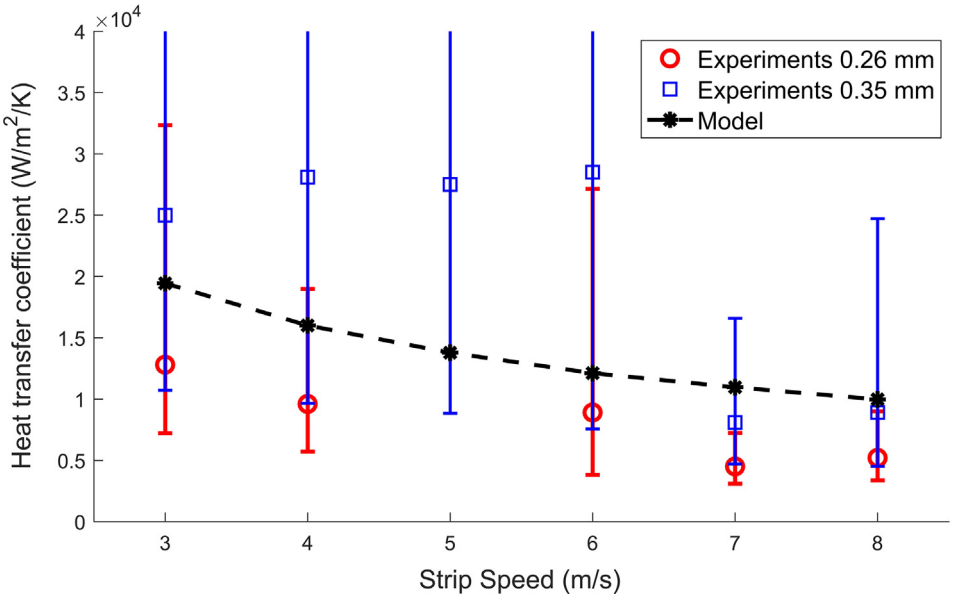

Fig. 8. Heat transfer coefficients with 72 kPa of radial stress applied by the strip to the heat pipe.

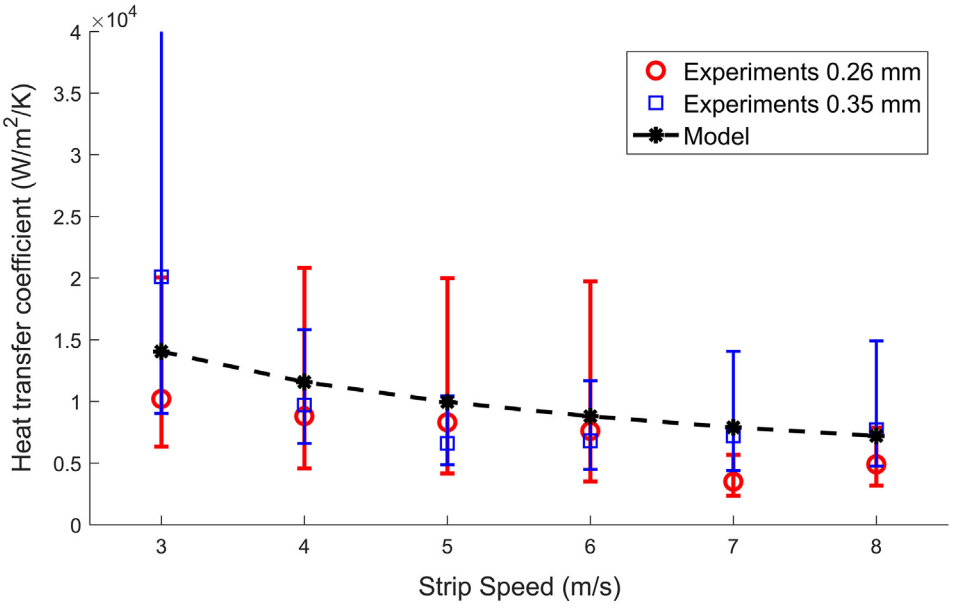

Fig. 9. Heat transfer coefficients with 48 kPa of radial stress applied by the strip to the heat pipe.

Figs. 8–10[2] for different radial stresses applied on the roll. It should be noted that in all of the cases, the gas layer thickness is computed to be larger than the effective roughness of the two surfaces. The contact pressure is therefore calculated as zero via Eq. (3). This results in a solid heat transfer coefficient of zero due to Eq. (25) because there is no physical contact between the surfaces. Conduction through the gas layer is the dominant term in the heat transfer coefficient.

The results show that the model is in very good agreement with the experimental results for low radial stress cases (Fig. 10). As the radial stress applied by the strip to the heat pipe doubles (Fig. 9), the difference between the experimental and modelling results as well as the magnitude of the error bars substantially increase. At the highest radial stress cases (Fig. 8), both the error bars and the difference between modelling and experimental results become very high. As previously explained, this is because the cases with lower contact heat transfer coefficient values give lower measurement errors and thus, are more precise.

When different data points in the same figure are compared, it is seen that the velocity increase causes the heat transfer to deteriorate. This trend is observed in the model as well as in the experiments. The reason for such a trend is an increase in the amount of gas entrained in the gap between the strip and the roll when the velocity is increased (see Eq. (1)). In order to satisfy the force balance shown in Eq. (2), the pressure of the entrained gas needs to remain constant. This results in an increase in the gas layer thick-

[2] The figures are plotted with the same scale to enable easier comparison. Due to large error bars for some of the cases, the y-axis of the plots (heat transfer coefficient values) is limited to a maximum of 40,000 W/m^2·K.

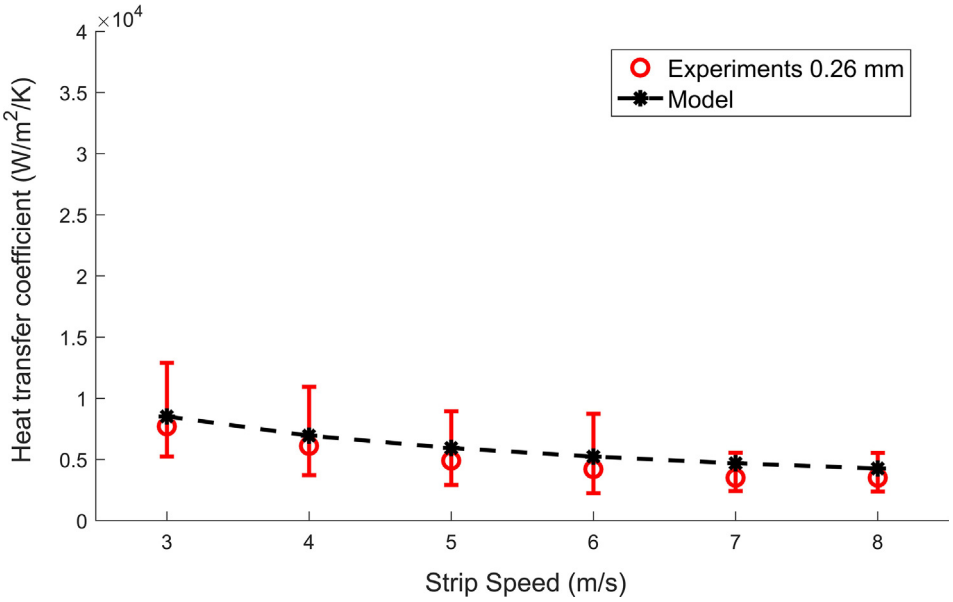

Fig. 10. Heat transfer coefficients with 24 kPa of radial stress applied by the strip to the heat pipe.

ness, *h*. A larger gas layer thickness results in a lower heat transfer coefficient, as shown in Eq. (26).

The effect of radial stress applied by the strip can be studied when the figures are compared to each other. An increase in the radial stress improves the contact heat transfer coefficient due to the decrease in gas layer thickness as per Eqs. (2) and (26). Using the numerical model, the highest heat transfer coefficient is calculated as 20,000 W/m^2·K for the 72 kPa radial stress and 3 m/s strip velocity case. The lowest heat transfer coefficient is calculated to be around 4000 W/m^2·K for the 24 kPa radial stress and 8 m/s strip velocity case.

The effect of radial stress and strip speed on heat transfer coefficient is summarized with a contour plot in Fig. 11.

In Fig. 11, the contour lines are obtained with the linear interpolation of the modelling results shown in Figs. 8–10. It is clearly seen that the heat transfer coefficient decreases with increasing speed and decreasing radial stress.

4.2. Other modelling results

During the experiments, the inlet region (A), where the heat transfer is expected to be limited, could not be discerned. This observation suggests that the extent of the inlet region (A) is relatively small. However, it is important to quantify it, as it reduces the uniform region and thus, the total heat transfer area.

At the inlet region (A), the strip approaches the heat pipe until a certain distance between the two surfaces is obtained. According to Eq. (2), the tension force and the ambient pressure are counterbalanced by the increasing entrained gas pressure and the contact pressure. Inlet region (A) grows with increasing strip velocity, decreasing strip specific tension and increasing strip thickness, as per the governing equations.

The numerical model results show that the inlet region (A) is always smaller than 1° out of 180° for the configurations shown in Fig. 5. Fig. 12 illustrates two such cases.

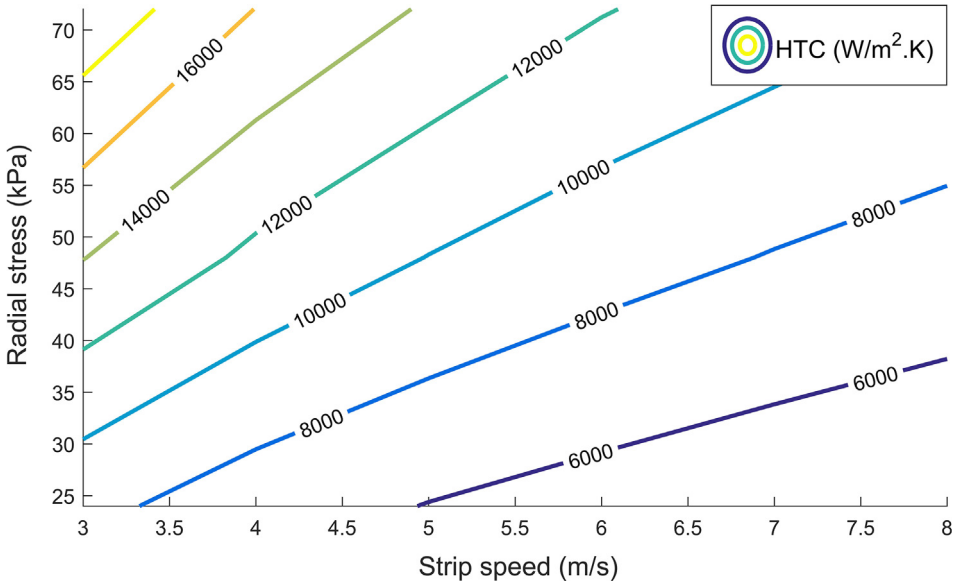

Fig. 11. Effect of strip speed and radial stress on heat transfer coefficient (HTC).

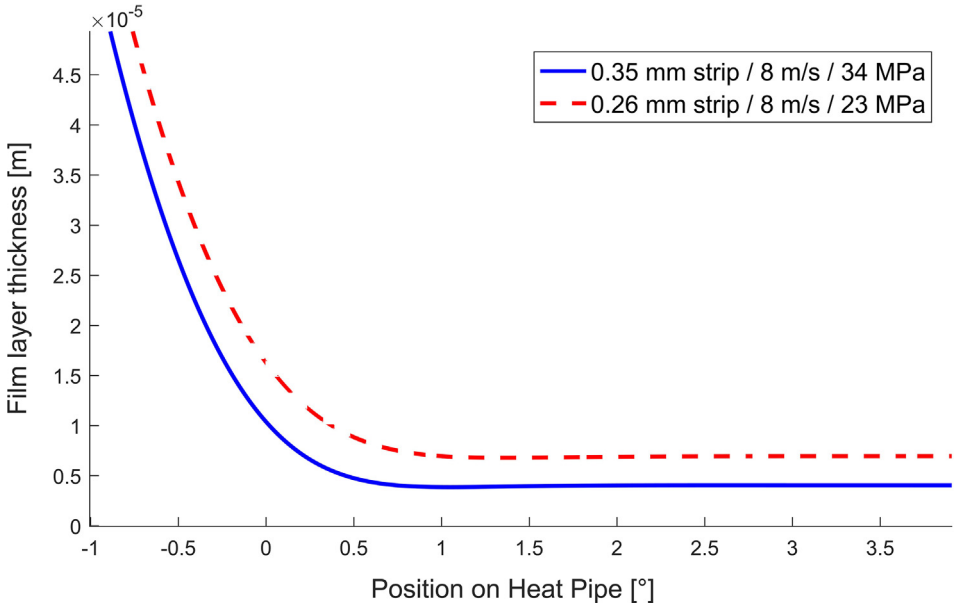

Fig. 12. Gas layer thickness at the inlet region (A).

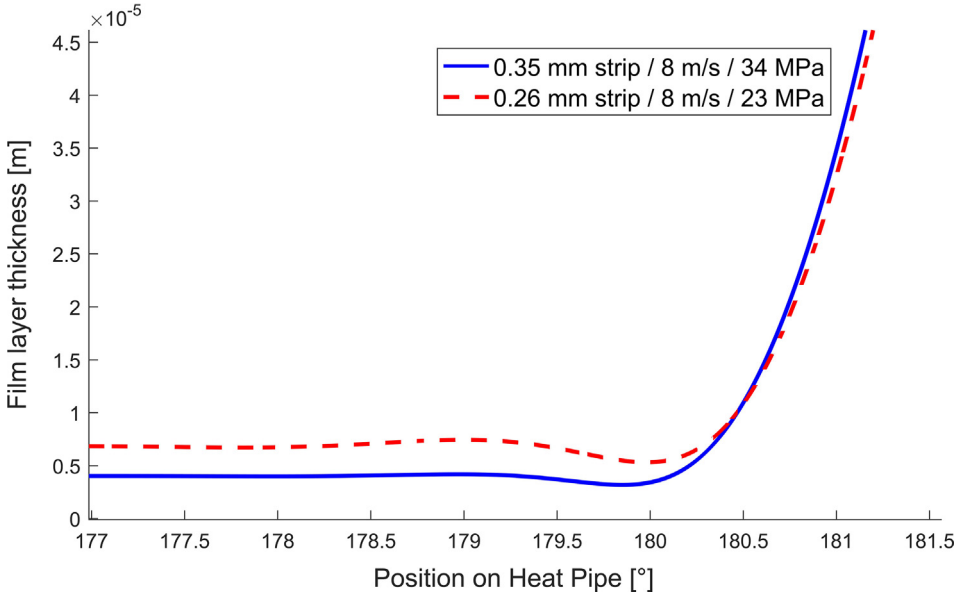

Fig. 13. Gas layer thickness at the outlet region (C).

The outlet region (C), on the other hand, was not in the field of view of the infrared camera during the experiments. The numerical model results also show that the outlet region (C) is always smaller than 1° out of 180° (see Fig. 13).[3]

The means that the uniform region (B) forms about 99% of the total contact area for all of the cases.

5. Conclusions

In this study, the contact heat transfer between a water containing rotating heat pipe and a moving steel strip is investigated. The determination of the contact heat transfer coefficient for different parameters is instrumental in the implementation of the heat pipe assisted annealing concept and valuable for other studies related to the heat transfer between a roll and a strip.

The results of this study show that the numerical model developed for strip to heat pipe contact is within the confidence limits of experiments. It is noted that the uncertainty of the measurements becomes very high when the heat transfer coefficient between the strip and the heat pipe is high.

The found heat transfer coefficient ranges from 4000 to 20,000 $W/m^2 \cdot K$, showing an increase with decreasing strip velocity and increasing radial stress. The heat transfer is dominated by gas conduction between the heat pipe and the strip. There is no solid heat transfer between the surfaces for the considered cases. The reduction of contact area due to strip bending and gas entrainment is found to be negligible for the examined cases.

Several improvements can be considered for the experimental part of this work. An additional measurement for the roll surface temperature or for the heat flux through the heat pipe shell would

[3] The undulation behavior seen at the outlet region is expected to be more visible with increasing stiffness [12]. However, in Fig. 13, the higher tension force applied to the thicker, and thus stiffer strip flattens this behavior.

provide less uncertainty in the experimental results. Moreover, the catalogue of reported heat transfer coefficient values can be extended with different entrained gas types and operating temperatures.

Acknowledgment

This work is part of a collaboration project between Tata Steel, TU Delft and Drever International.

The assistance of Cor Bijleveld, David Prins, Bastiaan de Bruijn and Stephan de Bruijn from the Strip Pilot Technology & Protoyping Group of Tata Steel and Michel Renard and Laurent Sturnack from Drever International is gratefully acknowledged.

References

[1] ASM Handbook Committee and American Society for Metals, Heat Treating. Materials Park, Ohio: American Society for Metals, 1991, pp. 42–55
[2] G. Paulussen, Corus Technology B. V., "Heat pipe assisted strip treatment," WO 2011012257 A1, 2011.
[3] G.M. Grover, T.P. Cotter, G.M. Erickson, Structures of very high thermal conductance, J. Appl. Phys. 35 (6) (Jun 1964) 1990–1991.
[4] P.D. Dunn and D. Reay, Heat Pipes. Elsevier, 2012, pp.135–169
[5] A. Faghri, Review and advances in heat pipe science and technology, J. Heat Transfer 134 (12) (Dec 2012) 123001.
[6] V. H. Gray, The rotating heat pipe-A wickless, hollow shaft for transferring high heat fluxes, in Proc. of ASME/AIChE Heat Transfer Conf., Minneapolis, USA, 1969.
[7] T.A. Jankowski, "Numerical and experimental investigations of a rotating heat pipe, Dissertation - The University of New Mexico, Albuquerque, New Mexico, 2007.
[8] L. Licht, Preliminary experiments with foil bearings, J. Basic Eng. 88 (1) (Mar. 1966) 1–3.
[9] L. Licht, An experimental study of elastohydrodynamic lubrication of foil bearings: part 1—displacement in the central zone, J. Lubr. Technol. 90 (1) (Jan. 1968) 199–220.
[10] A. Eshel, H.G. Elrod, The theory of the infinitely wide, perfectly flexible, self-acting foil bearing, J. Basic Eng. 87 (4) (Dec. 1965) 831–836.
[11] E.J. Barlow, Derivation of governing equations for self-acting foil bearings, J. Lubr. Technol. 89 (3) (Jul. 1967) 334–339.
[12] A. Eshel, H.G. Elrod, Stiffness effects on the infinitely wide foil bearing, J. Lubr. Technol. 89 (1) (Jan. 1967) 92–97.
[13] A. Eshel, Compressibility effects on the infinitely wide, perfectly flexible foil bearing, J. Lubr. Technol. 90 (1) (Jan. 1968) 221–225.
[14] M. Wildmann, Foil bearings, J. Lubr. Technol. 91 (1) (Jan. 1969) 37–44.
[15] C.A. Lacey, F.E. Talke, A tightly coupled numerical foil bearing solution, IEEE Trans. Magn. 26 (6) (Nov. 1990) 3039–3043.
[16] C. Lacey, F.E. Talke, Measurement and simulation of partial contact at the head/tape interface, J. Tribol. 114 (4) (Oct. 1992) 646–652.
[17] Y. Wu, F.E. Talke, The effect of surface roughness on the head-tape interface, J. Tribol. 118 (2) (Apr. 1996) 376–381.
[18] S. Müftü, R.C. Benson, A study of cross-width variations in the two-dimensional foil bearing problem, J. Tribol. 118 (2) (Apr. 1996) 407–414.
[19] S. Müftü, J.J. Jagodnik, Traction between a web and a smooth roller, J. Tribol. 126 (1) (Jan. 2004) 177–184.
[20] B.S. Rice, K.A. Cole, S. Müftü, A model for determining the asperity engagement height in relation to web traction over non-vented rollers, J. Tribol. 124 (3) (Jul. 2002) 584–594.
[21] M. M. Yovanovich, New contact and gap conductance correlations for conforming rough surfaces, in Proc. AIAA 16th Thermophysics Conf., Palo Alto, CA, 1981.
[22] G.S. Springer, Heat transfer in rarefied gases, Adv. Heat Transf. 7 (Dec. 1971) 163–218.
[23] S. Song, M.M. Yovanovich, F.O. Goodman, Thermal gap conductance of conforming surfaces in contact, J. Heat Transfer 115 (3) (Aug. 1993) 533–540.
[24] M.M. Yovanovich, Four decades of research on thermal contact, gap, and joint resistance in microelectronics, IEEE Trans. Compon. Packag. Technol. 28 (2) (Jun. 2005) 182–206.
[25] J.M. Buchlin, M. Delsipé, P. Planquart and M. Renard, Contact Conductance Determination using Infrared Thermography, in Quantitative Infrared Thermography Conf., Bordeaux, France, 2014
[26] M. Renard, J.M. Buchlin, Energy efficient strip annealing through roll regenerative furnace, Energy Procedia 120 (Aug. 2017) 380–387.
[27] J.M. Buchlin and M. Renard, Multi-roll heat exchanger, in Eurotherm Seminar 106, Paris, France, 2016
[28] N. Diomidis, J.P. Celis, P. Ponthiaux, F. Wenger, Tribocorrosion of stainless steel in sulfuric acid: identification of corrosion–wear components and effect of contact area, Wear 269 (1) (May 2010) 93–103.
[29] P. Colonna, and T. van der Stelt, FluidProp: A program for the estimation of thermophysical properties of fluids, Energy Technology Section, Delft University of Technology, The Netherlands.
[30] L. Bergman, F.P. Incropera, D.P. DeWitt, A.S. Lavine, Fundamentals of heat and mass transfer, John Wiley Sons (2011) 884–885.
[31] D.P. DeWitt, G.D. Nutter, Theory and Practice of Radiation Thermometry, Wiley, New York, 1988, pp. 987–989.
[32] W. Malalasekera and H. K. Versteeg. An introduction to computational fluid dynamics - The finite volume method. Harlow: Prentice Hall, 1995, pp.120-124
[33] R.J. Moffat, Describing the uncertainties in experimental results, Exp. Therm Fluid Sci. 1 (1) (Jan. 1988) 3–17.
[34] V.H. Gray, A.W. Joslyn and P.J. Marto, Boiling heat transfer coefficients, interface behavior, and vapor quality in rotating boiler operating to 475 G's, NASA Technical Notes, no. D-4136, Mar. 1968.